Chapter 19

Sorption of Molybdenum on Oxides, Clay Minerals, and Soils

Mechanisms and Models

Sabine Goldberg,[1] Chunming Su,[1,2] and Harold S. Forster[1]
[1]USDA-ARS, U.S. Salinity Laboratory, Riverside, California; [2]Presently at USEPA, National Risk Management Research Laboratory, Ada, OK

The constant capacitance model was well able to describe molybdate sorption on aluminum and iron oxides, clay minerals, and soils as a function of pH. The triple-layer model contained in version 3.1 of the program FITEQL was used to simultaneously optimize Mo surface complexation constants to Mo sorption data on goethite, gibbsite, δ-Al_2O_3, kaolinite, montmorillonite, and two arid-zone soils as a function of pH (3 to 10.5) and ionic strength (0.01, 0.1, and 1.0 mol·L^{-1} NaCl). This is a new capability for the FITEQL program, and the triple-layer model was well able to describe the ionic strength effects on all materials. Because of model sensitivity to the surface site density parameter, we used a surface site density value of 2.31 sites·nm^{-2}, which had been recommended by Davis and Kent (1990. *Rev. Mineral.* 23:117–260) for natural materials. Triple-layer modeling of Mo sorption was successful on all materials using this site density value. Use of a consistent site density value will facilitate the development of a self-consistent thermodynamic database, especially for heterogeneous natural sorbents such as clay minerals and soils.

I. INTRODUCTION

Molybdenum is a trace element required for both plant and animal nutrition. Molybdenum deficiencies are reported throughout the world for many agronomic crops, especially legumes (Murphy and Walsh, 1972). Molybdenum in its anionic form is readily taken up by forage plants and can accumulate to levels detrimental to grazing ruminant animals (Reisenauer *et al.*, 1962). To evaluate plant availability of Mo in soils, knowledge of its adsorption chemistry is required.

Molybdate adsorption has been investigated for a variety of soil minerals and soils. These adsorbent surfaces include aluminum oxides (Jones, 1957; Reisenauer *et al.*, 1962; Ferreiro *et al.*, 1985; Vordonis *et al.*, 1990; Spanos *et al.*, 1990a,b; Bibak and Borggaard, 1994; Spanos and Lycourghiotis, 1995; Goldberg *et al.*, 1996), iron oxides (Jones, 1957; Reisenauer *et al.*, 1962; Reyes and Jurinak, 1967; Kyriacou, 1967; McKenzie, 1983; Ferreiro *et al.*, 1985; Zhang and Sparks, 1989; Bibak and Borggaard, 1994; Goldberg *et al.*, 1996), clay minerals (Jones, 1957; Phelan and Mattigod, 1984; Mikkonen and Tummavuori, 1993a; Motta and Miranda, 1989; Goldberg *et al.*, 1996), and soils (Jones, 1957; Reisenauer *et al.*, 1962; Barrow, 1970; Theng, 1971; Gonzalez *et al.*, 1974; Jarrell and Dawson, 1978; Karimian and Cox, 1978; Roy *et al.*, 1986, 1989; Xie and MacKenzie, 1991; Xie *et al.*, 1993; Mikkonen and Tummavuori, 1993b; Goldberg *et al.*, 1996).

Molybdate adsorption on all of the above adsorbents increased with increasing solution pH from pH values of 2 to 4, exhibited a peak near pH 4, and decreased with increasing pH above pH 4. Aluminum and iron oxides represent important molybdate adsorbing surfaces in soils. Molybdate adsorption on soil clays dominant in kaolinite and illite was decreased by removal of amorphous aluminum and iron oxides (Theng, 1971). Molybdate adsorption in soils was highly correlated with extractable aluminum (Barrow, 1970) and iron (Gonzalez *et al.*, 1974; Jarrell and Dawson, 1978; Karimian and Cox, 1978), and drastically reduced after removal of amorphous iron oxides (Jones, 1957).

Ligand exchange is suggested to be the mechanism of molybdate adsorption on aluminum and iron oxide minerals (Jones, 1957; Ferreiro *et al.*, 1985). By this mechanism ions become adsorbed specifically as inner-sphere surface complexes. Inner-sphere surface complexes, by definition, contain no water molecules between the adsorbing ion and the surface functional group (Sposito, 1984). The point of zero charge (PZC) is defined as the pH value where there is no net particle charge (Sposito, 1984). Specific adsorption of anions onto variable-charge minerals, such as oxides, shifts the PZC to a more acid pH value. Molybdate adsorption lowered the PZC of goethite (McKenzie, 1983), amorphous iron oxide, δ-Al_2O_3, gibbsite, amorphous aluminum oxide, and kaolinites (Goldberg *et al.*, 1996), indicating specific adsorption on these minerals.

The dependence of ion adsorption on the effect of ionic strength has been used

to distinguish between inner- and outer-sphere surface complexes (Hayes and Leckie, 1987; Hayes *et al.*, 1988). Outer-sphere surface complexes, by definition, contain at least one water molecule between the adsorbing ion and the surface functional group (Sposito, 1984). Hayes *et al.* (1988) suggested that selenite, which showed little ionic strength dependence in its adsorption behavior, was specifically adsorbed on goethite in an inner-sphere surface complex, while selenate, which showed great ionic strength dependence, was adsorbed nonspecifically in an outer-sphere surface complex. Similarly, Zhang and Sparks (1989) found little ionic strength dependence of molybdate adsorption on goethite and interpreted this result as supporting evidence for inner-sphere surface complex formation.

The constant capacitance model (Stumm *et al.*, 1980) and the triple-layer model (Davis *et al.*, 1978) are chemical surface complexation models of the oxide–solution interface that use a ligand exchange mechanism to describe specific anion adsorption. These models explicitly define inner-sphere surface complexes and chemical reactions and consider the charge on both the adsorbate anion and the adsorbent surface. The constant capacitance model has been used successfully to describe molybdate adsorption on various aluminum and iron oxides via ligand exchange with surface hydroxyl groups and on various clay minerals via ligand exchange with aluminol groups as a function of solution pH (Goldberg *et al.*, 1996). The constant capacitance model has successfully described Mo adsorption on clay minerals as a function of equilibrium Mo concentration (Motta and Miranda, 1989). The constant capacitance model was unable to describe Mo adsorption on three soils as a function of solution pH (Goldberg *et al.*, 1996). The triple-layer model has been used successfully to describe molybdate adsorption on goethite as a function of solution pH (Zhang and Sparks, 1989).

The present study was initiated to reevaluate the ability of the constant capacitance model to describe molybdate adsorption behavior previously determined by Goldberg *et al.* (1996) on a variety of soils and soil minerals—Al oxide, Fe oxide, and clay minerals—as a function of solution pH. Molybdate adsorption on various adsorbents was evaluated as a function of solution pH and ionic strength in an effort to deduce adsorption mechanisms. The ability of the triple-layer model to describe all ionic strength data simultaneously with one set of molybdate surface complexation constants will also be investigated.

II. MATERIALS AND METHODS

Molybdenum adsorption behavior as a function of solution pH and ionic strength was studied on various adsorbents. δ-Al_2O_3, under the trade name Aluminium Oxid C, was obtained from Degussa (Teterboro, NJ). Goethite, α-FeOOH,

was synthesized as described by McLaughlin *et al.* (1981). Gibbsite, γ-$Al(OH)_3$, was synthesized according to the procedure of Kyle *et al.* (1975). No trace contaminants were observed in the oxides using X-ray diffraction analysis. Samples of KGa-1 kaolinite and SWy-1 montmorillonite were obtained from the Clay Minerals Society's Source Clays Repository (Univ. of Missouri, Columbia) and used without pretreatment. Surface samples of the Pachappa (coarse-loamy, mixed, thermic Mollic Haploxeralf) and Porterville (fine, montmorillonitic, thermic Typic Chromoxerert) soil series consisted of the <2-mm fraction. Organic and inorganic carbon analyses were carried out using the method of Nelson and Sommers (1982). Free aluminum and iron oxides were extracted as described by Coffin (1963).

Trace impurities in the oxides and clay minerals were determined using X-ray diffraction powder mounts (see Table I). To obtain dominant clay mineralogy of the soils, X-ray diffraction peak areas obtained using oriented mounts were converted directly to clay mineral contents as described by Klages and Hopper (1982). Specific surface areas of the clay minerals and oxides were determined with a single-point BET N_2 adsorption isotherm obtained using a Quantasorb Jr. surface area analyzer (Quantachrome Corp., Syosset, NY). Specific surface areas of the soil samples were obtained using ethylene glycol monoethylether (EGME) adsorption as described by Cihacek and Bremner (1979). Points of zero charge and electrophoretic mobilities were determined for all oxides and kaolinite by microelectrophoresis as described by Goldberg *et al.* (1996). Table I presents point of zero charge and specific surface area data for the oxides and clay minerals. Table II presents chemical, mineralogical, and specific surface area data for the soils.

Molybdate adsorption experiments were carried out in batch systems to determine adsorption envelopes (amount of Mo adsorbed as a function of solution pH per fixed total Mo concentration). Samples of adsorbent were added to 50-ml polypropylene centrifuge tubes or 250-ml centrifuge bottles and equilibrated with aliquots (see Table III for solids concentration) of a 0.01, 0.1, or 1.0 $mol \cdot L^{-1}$ NaCl solution by shaking for 20 hr on a reciprocating shaker at 23 ± 1°C. This solution

Table I

Characterization of Oxides and Clay Minerals

Solid	Surface area ($m^2 \cdot g^{-1}$)	Point of zero charge
Goethite	63.7	8.82
δ-Al_2O_3	102.9	9.30
Gibbsite	56.5	9.41
KGa-1 kaolinite	9.14	2.88
SWy-1 montmorillonite	18.6	

Table II

Characterization of Soils

Soil	Inorganic carbon (%)	Organic carbon (%)	Free aluminum (%)	Free iron (%)	Surface area ($m^2 \cdot g^{-1}$)	Dominant minerals
Pachappa	0.010	0.49	0.067	0.76	36.3	Illite, kaolinite, montmorillonite
Porterville	0.023	0.84	0.090	1.07	172.2	Kaolinite, illite, montmorillonite

Table III

Solids Concentrations and Intrinsic Surface Complexation Constants Obtained with the Constant Capacitance Model

Solid	Solids concentration ($g \cdot L^{-1}$)	log K_+(int)	log K_-(int)	log K^1_{Mo}(int)	log K^2_{Mo}(int)
Iron oxides					
Hematite	5.0	7.31	−8.80	8.71	3.44
Goethite	1.25	7.31	−8.80	8.54	1.13
Poorly crystallized goethite	0.64	7.31	−8.80	9.51	3.10
Amorphous iron oxide	0.64	7.31	−8.80	9.72	2.75
Average (iron oxides)				8.99 ± 0.64	2.33 ± 1.05
Aluminum oxides					
δ-Al_2O_3	4.0	7.38	−9.09	9.61	—[a]
Gibbsite	1.25	7.38	−9.09	8.93	1.60
Amorphous aluminum oxide	0.35	7.38	−9.09	9.37	2.89
Average (aluminum oxides)				9.30 ± 0.34	2.25 ± 0.91
Average (oxides)				9.15 ± 0.49	2.29 ± 0.87
Clays					
KGa-1 kaolinite	200	4.95	−9.09	7.68	—
KGa-2 kaolinite	100	5.99	−9.09	8.69	—
SWy-1 montmorillonite	30	7.38	−9.09	8.43	0.62
SAz-1 montmorillonite	40	3.83	−1.26	8.36	—
STx-1 montmorillonite	40	2.81	−9.09	5.41	—
IMt-illite	50	7.38	−9.09	8.79	—
Average (clays)				7.89 ± 1.28	
Soils					
Hesperia soil	200	7.35	−8.95	8.28	0.63
Pachappa soil	200	7.35	−8.95	9.36	1.20
Porterville soil	200	7.35	−8.95	9.00	2.04
Average (soils)				8.88 ± 0.55	1.29 ± 0.71

[a]No convergence.

contained 0.292 mol·m^{-3} of Mo from $Na_2MoO_4 \cdot 2H_2O$ (Mallinckrodt, Inc., St. Louis, MO) and had been adjusted to the desired pH values using 1.0 mol·L^{-1} HCl or 1.0 mol·L^{-1} NaOH additions that changed the total volume by ≤2%. Experiments were carried out at 0.292 mol·m^{-3} of Mo to avoid the formation of Mo polymers in solution (Carpéni, 1947). The samples were centrifuged at a relative centrifugal force of 7800*g* for 20 min. The decantates were analyzed for pH, filtered through a 0.45-μm Whatman filter, and analyzed for Mo concentration with inductively coupled plasma (ICP) emission spectrometry.

In situ attenuated total reflectance Fourier transform infrared (ATR-FTIR) spectroscopy and diffuse reflectance infrared Fourier transform (DRIFT) spectroscopy were used to study sorption of Mo on a synthetic amorphous iron oxide, $Fe(OH)_3$(a), described by Su and Suarez (1995). Amorphous iron oxide was chosen because it is known to sorb large amounts of Mo, and it does not exhibit strong infrared (IR) absorbance in the region where Mo shows characteristic IR bands. Amorphous iron oxide has a BET N_2 surface area of 250 m^2·g^{-1}. The suspensions of $Fe(OH)_3$(a) were prepared by adding 2.0 g of solids to each 20 ml of 1.0 mol·L^{-1} NaCl (pH 6), 0.05 mol·L^{-1} Na_2MoO_4 + 1.0 mol·L^{-1} NaCl (pH 6), or 1.0 mol·L^{-1} Na_2MoO_4 + 1.0 mol·L^{-1} NaCl (pH 6). Suspension pH was maintained at 6 by frequent additions of 1.0 mol·L^{-1} NaOH or 1.0 mol·L^{-1} HCl. The suspensions were shaken for 24 hr at ambient temperature and centrifuged. Fifteen milliliters of the supernatant were removed and a 3.5-ml subsample was used as the reference in the ATR-FTIR study. The solid was resuspended in the remaining 5 ml of supernatant and used as the sample. A solid concentration of 400 g·L^{-1} was achieved in the sampling ATR reservoir. Concentrations of Mo in the supernatant were determined by ICP.

Infrared spectra of the aqueous solutions of 1.0 mol·L^{-1} NaCl (pH 6) and 0.05 and 0.10 mol·L^{-1} Na_2MoO_4 + 1.0 mol·L^{-1} NaCl (pH 6), and the suspensions of $Fe(OH)_3$(a) reacted with Mo, were recorded in the 4000 to 7000 cm^{-1} range using a Bio-Rad Digilab FTS-7 spectrometer (Bio-Rad Digilab Div., Cambridge, MA). The ATR accessory consisted of a horizontal reservoir and a ZnSe crystal rod with a 45° angle of incidence. Single-beam IR spectra were obtained from 2000 scans using a resolution of 4 cm^{-1}. All final spectra were the results of subtracting the spectrum of the supernatant or of 1.0 mol·L^{-1} NaCl (pH 6) from the spectrum of the $Fe(OH)_3$(a) suspensions or of 0.05 and 0.10 mol·L^{-1} Na_2MoO_4 + 1.0 mol·L^{-1} NaCl (pH 6), respectively. A subtraction factor of unity was always used.

A subsample of 1.0 ml of the solid suspension (400 g·L^{-1}) was washed twice with 30 ml of deionized water and air dried before DRIFT spectroscopic analysis. DRIFT spectra of samples diluted with KBr (5-mg sample in 95 mg KBr) were recorded from 4000 to 200 cm^{-1} at 4 cm^{-1} resolution over 500 scans. A subsample of the washed solids was examined by X-ray diffraction and subsequently dissolved in 0.5 mol·L^{-1} HNO_3 and analyzed for Mo concentration by ICP.

A. Constant Capacitance Modeling

The constant capacitance model (Stumm *et al.*, 1980) was used to describe molybdate adsorption behavior on the adsorbents as a function of solution pH in a background electrolyte of 0.1 mol·L^{-1} NaCl. The computer program FITEQL, version 3.1 (Herbelin and Westall, 1994), had been used to fit intrinsic molybdate surface complexation constants to the experimental adsorption data as presented in Goldberg *et al.* (1996). In the present study the data from Goldberg *et al.* (1996) are reanalyzed using Mo (ads) as a "dummy" component. Using this procedure, we obtained an improved fit and were able to use the preprocessor graphing routine to check the goodness-of-fit of the model to the data. Additional explanation on the use of the adsorbed ion as a "dummy" component is provided by Herbelin and Westall (1994).

Molybdenum occurs as MoO_4^{2-} over most of the pH range. The acid–base reactions undergone by molybdic acid are

$$H_2MoO_{4(aq)} \rightleftarrows H^+_{(aq)} + HMoO^-_{4(aq)} \quad [1]$$

$$H_2MoO_{4(aq)} \rightleftarrows 2H^+_{(aq)} + MoO^{2-}_{4(aq)}, \quad [2]$$

with pK values of 4.00 and 8.24, respectively (Lindsay, 1979).

In the constant capacitance model the protonation and dissociation reactions for the surface functional group, SOH (where SOH represents a reactive surface hydroxyl bound to a metal ion, S (Al or Fe), in the oxide mineral or an aluminol at the clay mineral edge), are defined as

$$SOH_{(s)} + H^+_{(aq)} \rightleftarrows SOH^+_{2(s)} \quad [3]$$

$$SOH_{(s)} \rightleftarrows SO^-_{(s)} + H^+_{(aq)}. \quad [4]$$

The constant capacitance model contains the assumption that all surface complexes are inner-sphere. Therefore the surface complexation reactions for molybdate adsorption are defined as

$$SOH_{(s)} + H_2MoO_{4(aq)} \rightleftarrows SHMoO_{4(s)} + H_2O \quad [5]$$

$$SOH_{(s)} + H_2MoO_{4(aq)} \rightleftarrows SMoO^-_{4(s)} + H^+_{(aq)} + H_2O. \quad [6]$$

The intrinsic equilibrium constants for protonation and dissociation reactions of the surface functional group are

$$K_+(\text{int}) = \frac{[SOH_2^+]}{[SOH][H^+]} \exp(F\psi_o/RT) \quad [7]$$

$$K_-(\text{int}) = \frac{[SO^-][H^+]}{[SOH]} \exp(-F\psi_o/RT), \quad [8]$$

where F is the Faraday constant (C·mol$_c^{-1}$), ψ_o is the surface potential (V), o refers to the surface plane of adsorption, R is the molar gas constant (J·mol^{-1}·K^{-1}), T

is the absolute temperature (K), and square brackets represent concentrations ($mol \cdot L^{-1}$). The intrinsic equilibrium constants for the molybdate surface complexation reactions are

$$K^{1s}_{Mo}(int) = \frac{[SHMoO_4]}{[SOH][H_2MoO_4]} \quad [9]$$

$$K^{2s}_{Mo}(int) = \frac{[SMoO_4^-][H^+]}{[SOH][H_2MoO_4]} \exp(-F\psi_o/RT), \quad [10]$$

where the subscript "is" refers to inner-sphere surface complexation.

The mass balance expression for the surface functional group is

$$[SOH]_T = [SOH] + [SOH_2^+] + [SO^-] + [SHMoO_4] + [SMoO_4^-] \quad [11]$$

where $[SOH]_T$ is related to the surface site density, N_s, by

$$[SOH]_T = \frac{S_A C_p 10^{18}}{N_A} N_s, \quad [12]$$

where S_A is the surface area ($m^2 \cdot g^{-1}$), C_p is the solids concentration ($g \cdot L^{-1}$), N_A is Avogadro's number, and N_s has units of sites$\cdot nm^{-2}$.

The charge balance expression is

$$\sigma_o = [SOH_2^+] - [SO^-] - [SMoO_4^-], \quad [13]$$

where σ_o represents the surface charge ($mol_c \cdot L^{-1}$). The relationship between surface charge and surface potential is

$$\sigma_o = \frac{\boldsymbol{C} S_A C_p}{F} \psi_o \quad [14]$$

where $\boldsymbol{C}$ is the capacitance ($F \cdot m^{-2}$).

In our application of the constant capacitance model, the surface site density was treated as molybdate reactive site density and set to the maximum Mo adsorption obtained in our experiments. Numerical values of the intrinsic protonation constant, $K_+(int)$, and the intrinsic dissociation constant, $K_-(int)$, were obtained from the literature compilation of experimental values for aluminum and iron oxides of Goldberg and Sposito (1984a). The intrinsic protonation and dissociation constants were initially fixed at log $K_+(int) = 7.31$ and log $K_-(int) = -8.80$ for goethite; log $K_+(int) = 7.38$ and log $K_-(int) = -9.09$ for gibbsite and the clays (Goldberg and Sposito, 1984a); and log $K_+(int) = 7.35$ and log $K_-(int) = -8.95$ for the soils (Goldberg and Sposito, 1984b). For the kaolinites and two of the montmorillonites it was subsequently necessary to optimize log $K_+(int)$ or log $K_+(int)$ and log $K_-(int)$ as well as the molybdate surface complexation constants using the FITEQL program. The capacitance density was fixed at $\boldsymbol{C} = 1.06$ $F \cdot m^{-2}$, considered optimum for γ-Al_2O_3 by Westall and Hohl (1980). It is prefer-

able to minimize the number of adjustable parameters by obtaining values of log K_+(int) and log K_-(int) experimentally from titration data when available.

The goodness-of-fit criterion is the overall variance, V, in Y (Herbelin and Westall, 1994),

$$V_Y = \frac{SOS}{DF}, \qquad [15]$$

where SOS is the weighted sum of squares of the residuals and DF is the degrees of freedom.

B. Triple-Layer Modeling

The triple-layer model allows ion adsorption as either inner-sphere or outer-sphere surface complexes. In addition to the protonation–dissociation reactions, Eqs. [3] and [4], the triple-layer model considers outer-sphere surface complexation reactions for the background electrolyte:

$$SOH_{(s)} + Na^+_{(aq)} \rightleftarrows SO^- - Na^+_{(s)} + H^+_{(aq)} \qquad [16]$$

$$SOH_{(s)} + H^+_{(aq)} + Cl^-_{(aq)} \rightleftarrows SOH_2^+ - Cl^-_{(s)}. \qquad [17]$$

In the triple-layer model, inner-sphere surface complexation reactions and intrinsic equilibrium constant expressions for molybdate are given by Eqs. [5], [6], [9], and [10], as for the constant capacitance model. The outer-sphere surface complexation reactions for molybdate adsorption are

$$SOH_{(s)} + H_2MoO_{4(aq)} \rightleftarrows SOH_2^+ - HMoO^-_{4(s)} \qquad [18]$$

$$SOH_{(s)} + H_2MoO_{4(aq)} \rightleftarrows SOH_2^+ - MoO^{2-}_{4(s)} + H^+_{(aq)}. \qquad [19]$$

The intrinsic equilibrium constants for outer-sphere surface complexation are

$$K_{Na+}(int) = \frac{[SO^- - Na^+][H^+]}{[SOH][Na^+]} \exp[F(\psi_\beta - \psi_o)/RT] \qquad [20]$$

$$K_{Cl-}(int) = \frac{[SOH_2^+ - Cl^-]}{[SOH][H^+][Cl^-]} \exp[F(\psi_o - \psi_\beta)/RT] \qquad [21]$$

$$K^{1os}_{Mo}(int) = \frac{[SOH_2^+ - HMoO_4^-]}{[SOH][H_2MoO_4]} \exp[F(\psi_o - \psi_\beta)/RT] \qquad [22]$$

$$K^{2os}_{Mo}(int) = \frac{[SOH_2^+ - MoO_4^{2-}][H^+]}{[SOH][H_2MoO_4]} \exp[F(\psi_o - 2\psi_\beta)/RT], \qquad [23]$$

where β refers to the plane of outer-sphere adsorption and the subscript "os" refers to outer-sphere surface complexation.

The mass balance for the surface functional group is

$$[SOH]_T = [SOH] + [SOH_2^+] + [SO^-] + [SHMoO_4] + [SMoO_4^-] + [SOH_2^+\text{–}HMoO_4^-] + [SOH_2^+\text{–}MoO_4^{2-}] + [SO^-\text{–}Na^+] + [SOH_2^+\text{–}Cl^-]. \quad [24]$$

The charge balance expressions are

$$\sigma_o + \sigma_\beta + \sigma_d = 0 \quad [25]$$

$$\sigma_o = [SOH_2^+] + [SOH_2^+\text{–}HMoO_4^-] + [SOH_2^+\text{–}MoO_4^{2-}] + [SOH_2^+\text{–}Cl^-] - [SO^-] - [SOMoO_4^-] - [SO^-\text{–}Na^+] \quad [26]$$

$$\sigma_\beta = [SO^-\text{–}Na^+] - [SOH_2^+\text{–}HMoO_4^-] - 2[SOH_2^+\text{–}MoO_4^{2-}] - [SOH_2^+\text{–}Cl^-]. \quad [27]$$

The relationships between the surface charges and the surface potentials are

$$\sigma_o = \frac{C_1 S_A C_p}{F} (\psi_o - \psi_\beta) \quad [28]$$

$$\sigma_d = \frac{C_2 S_A C_p}{F} (\psi_d - \psi_\beta) \quad [29]$$

$$\sigma_d = \frac{S_A C_p}{F} (8\epsilon_o DRT\boldsymbol{I})^{1/2} \sinh(F\psi_d/2RT), \quad [30]$$

where $\boldsymbol{C}_1$ and $\boldsymbol{C}_2$ are capacitances, d refers to the plane of the diffuse ion swarm, ϵ_o is the permittivity of vacuum, D is the dielectric constant of water, and $\boldsymbol{I}$ is the ionic strength.

The surface site density was set at a value of 2.31 sites·nm^{-2}. This value had been recommended by Davis and Kent (1990) for natural materials. Numerical values for the intrinsic protonation and dissociation constants and the surface complexation constants were obtained from the literature. For goethite these constants were log K_+(int) = 4.3, log K_-(int) = −9.8, log K_{Na^+}(int) = −9.3, and log K_{Cl^-}(int) = 5.4, as obtained by Zhang and Sparks (1990). For aluminum oxides, clays, and soils these constants were log K_+(int) = 5.0, log K_-(int) = −11.2, log K_{Na^+}(int) = −8.6, and log K_{Cl^-}(int) = 7.5, as obtained by Sprycha (1989a,b) on γ-Al_2O_3. Molybdate surface complexation constants were fit simultaneously to the adsorption data at three different ionic strengths using either inner-sphere or outer-sphere adsorption mechanisms. For δ-Al_2O_3 and clays, and gibbsite with an outer-sphere adsorption mechanism, it was subsequently necessary to optimize log K_{Na^+}(int) and log K_{Cl^-}(int) as well as the molybdate surface complexation constants using the FITEQL program. The capacitances were fixed at $\boldsymbol{C}_1$ = 1.2 F·m^{-2} and $\boldsymbol{C}_2$ = 0.2 F·m^{-2}, values considered optimum for goethite by Zhang and Sparks (1990). It is preferable to minimize the number of adjustable parameters by ob-

taining values of log K_+(int), log K_-(int), log K_{Na^+}(int), and log K_{Cl^-}(int) experimentally from titration data when available.

III. RESULTS AND DISCUSSION

The fit of the constant capacitance model to the data of Goldberg *et al.* (1996) using Mo(ads) as a "dummy" component is indicated in Figures 1 to 5. Molybdate adsorption on all materials exhibited a maximum at low pH (3 to 5). With increasing solution pH, adsorption decreased rapidly, with little adsorption occurring above pH values of 7 to 8. The constant capacitance model was well able to describe molybdate adsorption on all iron and aluminum oxides studied, with some deviations occurring at low and high pH values (Figs. 1 and 2). Use of Mo(ads) as a "dummy" component improved the model fit for all oxides except amorphous iron and aluminum oxide (compare Figs. 1 and 2 to Figs. 4 and 5 of Goldberg *et al.* (1996)). Molybdate adsorption on the oxides was described with the model when only the molybdate surface complexation constants, K^1_{Mo}(int) and K^2_{Mo}(int), were optimized.

The constant capacitance model was well able to describe molybdate adsorp-

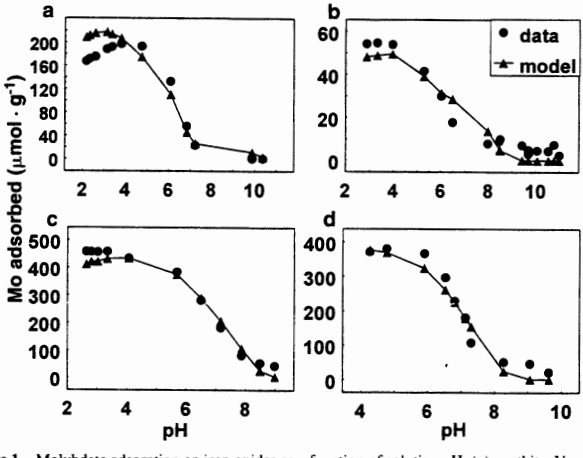

Figure 1 Molybdate adsorption on iron oxides as a function of solution pH: (a) goethite, V_Y = 106; (b) hematite, V_Y = 312; (c) poorly crystallized goethite, V_Y = 85.9; (d) amorphous iron oxide, V_Y = 112. Circles represent experimental data. Model results are represented by triangles and solid lines.

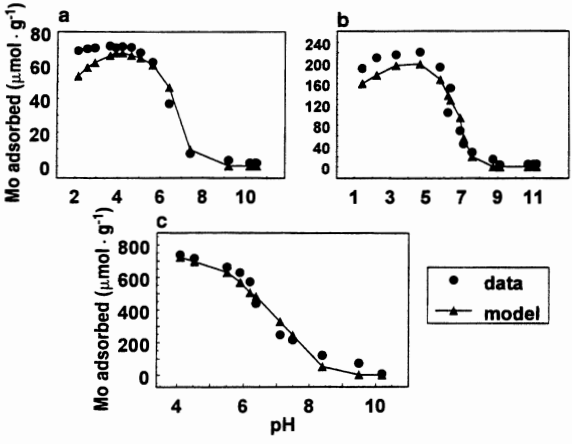

Figure 2 Molybdate adsorption on aluminum oxides as a function of solution pH: (a) δ-Al_2O_3, V_Y = 67.3; (b) gibbsite, V_Y = 92.5; (c) amorphous aluminum oxide, V_Y = 111. Circles represent experimental data. Constant capacitance model results are represented by triangles and solid lines.

tion on the kaolinites with no improvement observed by use of the "dummy" component (compare Fig. 3 to Figs. 6a and 6b of Goldberg *et al.* (1996)). The ability of the model to describe molybdate adsorption on 2:1 clay minerals is indicated in Figure 4. Use of the "dummy" component improved the fit for SAz-1 and STx-1 montmorillonite, and degraded it for SWy-1 montmorillonite and IMt-1 illite (compare Fig. 4 to Figs. 6c, 6d, 6e, and 6f of Goldberg *et al.* (1996)). However, this latter comparison is deceptive because unlike in the previous study (Goldberg *et al.*, 1996), log K_+(int) and log K_-(int) were not optimized for SWy-1 montmorillonite and IMt-1 illite. log K_+(int) was optimized along with the molybdate surface complexation constants in describing adsorption on the kaolinites and the STx-1 montmorillonite. For the SAz-1 montmorillonite, log K_-(int) was optimized as well.

The constant capacitance model was able to describe molybdate adsorption on the three soils studied with some deviations occurring especially at low pH values (Fig. 5). The model was unable to describe molybdate adsorption on the Hesperia soil below pH 4 where large deviations from the data were observed. In their application of the model, Goldberg *et al.* (1996) were unable to describe any of the soil data since convergence of the FITEQL computer program (Herbelin and Westall, 1994) either could not be obtained or provided a very bad fit.

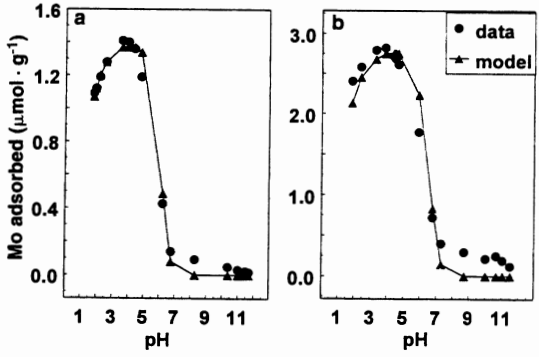

Figure 3 Molybdate adsorption on kaolinites as a function of solution pH: (a) KGa-1 kaolinite, V_Y = 38.7; (b) KGa-2 kaolinite, V_Y = 155. Circles represent experimental data. Constant capacitance model results are represented by triangles and solid lines.

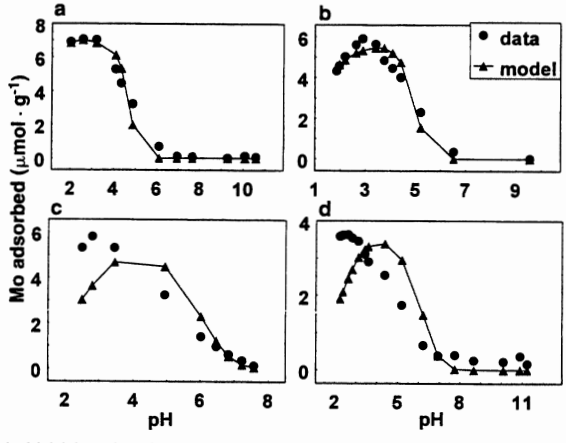

Figure 4 Molybdate adsorption on 2:1 clay minerals as a function of solution pH: (a) SAz-1 montmorillonite, V_Y = 96.1; (b) STx-1 montmorillonite, V_Y = 64.4; (c) SWy-1 montmorillonite, V_Y = 271; (d) IMt-1 illite, V_Y = 327. Circles represent experimental data. Constant capacitance model results are represented by triangles and solid lines.

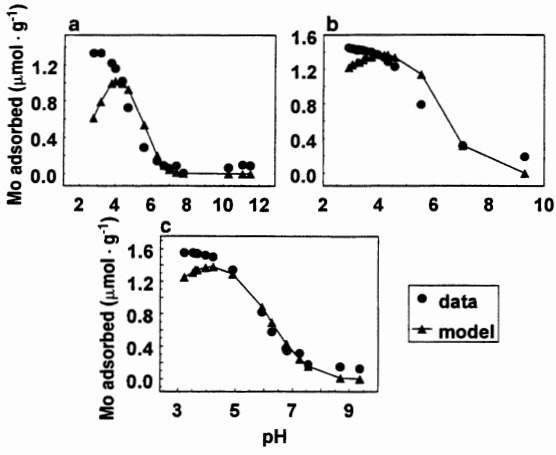

Figure 5 Molybdate adsorption on soils as a function of solution pH: (a) Hesperia, V_Y = 324; (b) Pachappa, V_Y = 147; (c) Porterville, V_Y = 125. Circles represent experimental data. Constant capacitance model results are represented by triangles and solid lines.

Table III provides values of the molybdate surface complexation constants obtained using the constant capacitance model in the FITEQL program for all materials. To fit the molybdate adsorption data we never optimized more than two adjustable parameters for any adsorbent. This number of adjustable parameters compares very favorably with the empirical Langmuir and Freundlich adsorption isotherm approach. The good fit of the model to molybdate adsorption on oxides, kaolinites, two of the clay minerals, and two of the soils suggests that inner-sphere surface complexation is the appropriate adsorption mechanism for these materials. The numerical values of the molybdate surface complexation constants for these materials were similar in magnitude (see Table III). Averages for the molybdate surface complexation constants obtained with the constant capacitance model for aluminum oxides, iron oxides, clay minerals, and soils were not statistically different at the 95% level of confidence, suggesting a common adsorption mechanism.

The effect of ionic strength on molybdate adsorption on a variety of adsorbents is indicated in Figures 6 to 12. Solution ionic strength was varied by two orders of magnitude, from 0.01 to 1.0 mol·L^{-1} NaCl. On all materials, adsorption of molybdate was consistently lowest for the highest ionic strength. The adsorbents exhibited diverse behavior in their ionic strength dependence. Goethite and montmorillonite showed relatively little ionic strength dependence, suggesting the formation

of inner-sphere surface complexes. An inner-sphere adsorption mechanism for goethite had already been indicated by the electrophoretic mobility measurements of Goldberg *et al.* (1996). The soils showed little ionic strength dependence except at both low and high pH values. Gibbsite, δ-Al_2O_3, and kaolinite exhibited obvious ionic strength dependence. However, this behavior is in contradiction to the inner-sphere adsorption mechanism suggested for these materials by the electrophoretic mobility results of Goldberg *et al.* (1996). This discrepancy highlights the limitation in relying on macroscopic chemical information to deduce ion adsorption mechanisms.

The triple-layer model was used to describe the adsorption of molybdate on goethite, gibbsite, δ-Al_2O_3, KGa-1 kaolinite, SWy-1 montmorillonite, and two soils as a function of solution pH and ionic strength. All ionic strength and pH data were optimized simultaneously. Figures 6 to 12 indicate the ability of the triple-layer model to describe molybdate adsorption using both an inner-sphere and an outer-sphere adsorption mechanism. The surface site density and the capacitances were set at identical values for all adsorbents. Log K_{-}(int) and log K_{-}(int) values were obtained from the literature and set at identical values for all materials having AlOH as the reactive functional group (i.e., gibbsite, δ-Al_2O_3, kaolinite, montmorillonite, and soils). Different values were used for the goethite having FeOH as the reactive functional group.

The ability of the triple-layer model to describe molybdate adsorption on

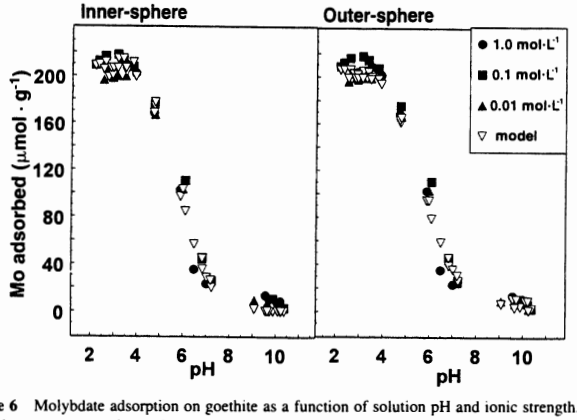

Figure 6 Molybdate adsorption on goethite as a function of solution pH and ionic strength. Filled symbols represent experimental data. Triple-layer model results are represented by open triangles. V_Y = 39.7 for inner-sphere adsorption and V_Y = 29.1 for outer-sphere adsorption.

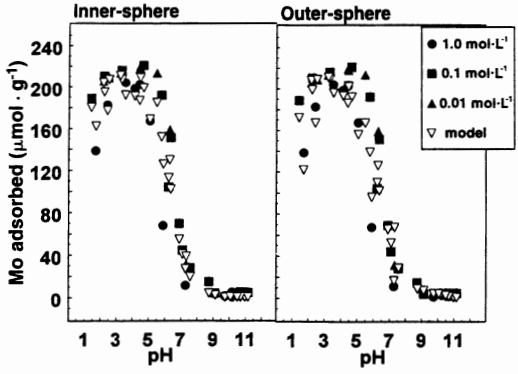

Figure 7 Molybdate adsorption on gibbsite as a function of solution pH and ionic strength. Filled symbols represent experimental data. Triple-layer model results are represented by open triangles. V_Y = 83.9 for inner-sphere adsorption and V_Y = 81.8 for outer-sphere adsorption.

goethite and gibbsite is presented in Figures 6 and 7, respectively. For both oxides the fit of the model was improved using the inner-sphere adsorption mechanism. For goethite this result is in agreement with the electrophoretic mobility and ionic strength results. For gibbsite the ionic strength effect data suggest an outer-sphere adsorption mechanism, in contrast to the modeling and electrophoretic mobility results. For δ-Al_2O_3 the quality of the triple-layer model fit is comparable for inner-sphere and outer-sphere adsorption mechanisms (Fig. 8).

Figures 9 and 10 present the ability of the triple-layer model to describe molybdate adsorption on kaolinite and montmorillonite, respectively. For kaolinite the quality of the model fit is improved using an inner-sphere adsorption mechanism (Fig. 9). This result is in agreement with the electrophoretic mobility results but contradicts the ionic strength dependence data. For montmorillonite an acceptable model fit could be obtained only using an outer-sphere adsorption mechanism (Fig. 10). This finding is in contradiction with the inner-sphere adsorption mechanism implied by the small ionic strength dependence of the adsorption data. For the soils (Figs. 11 and 12), the quality of the model fit is slightly better for the inner-sphere adsorption mechanism, in agreement with the small ionic strength dependence in the intermediate pH range.

Table IV provides values of the molybdate inner- and outer-sphere surface complexation constants obtained using the triple-layer model in the FITEQL program for all materials. For goethite with both mechanisms, and for gibbsite using an in-

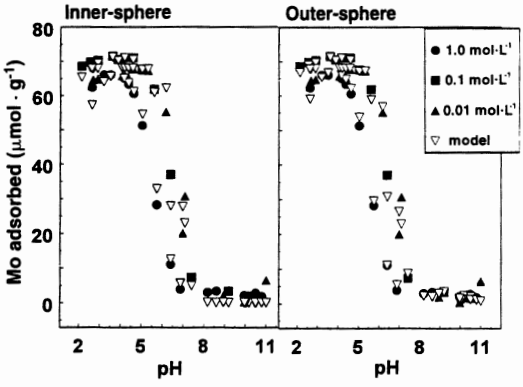

Figure 8 Molybdate adsorption on δ-Al_2O_3 as a function of solution pH and ionic strength. Filled symbols represent experimental data. Triple-layer model results are represented by open triangles. V_Y = 44.3 for inner-sphere adsorption and V_Y = 20.7 for outer-sphere adsorption.

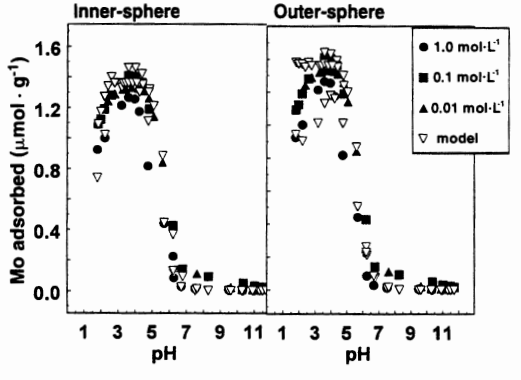

Figure 9 Molybdate adsorption on KGa-1 kaolinite as a function of solution pH and ionic strength. Filled symbols represent experimental data. Triple-layer model results are represented by open triangles. V_Y = 35.6 for inner-sphere adsorption and V_Y = 47.0 for outer-sphere adsorption.

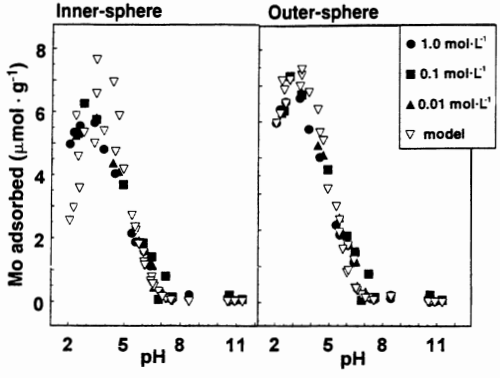

Figure 10 Molybdate adsorption on SWy-1 montmorillonite as a function of solution pH and ionic strength. Filled symbols represent experimental data. Triple-layer model results are represented by open triangles. V_Y = 146 for inner-sphere adsorption and V_Y = 76.0 for outer-sphere adsorption.

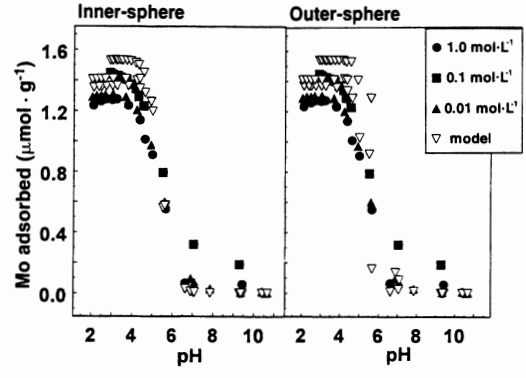

Figure 11 Molybdate adsorption on Pachappa soil as a function of solution pH and ionic strength. Filled symbols represent experimental data. Triple-layer model results are represented by open triangles. V_Y = 93.0 for inner-sphere adsorption and V_Y = 131 for outer-sphere adsorption.

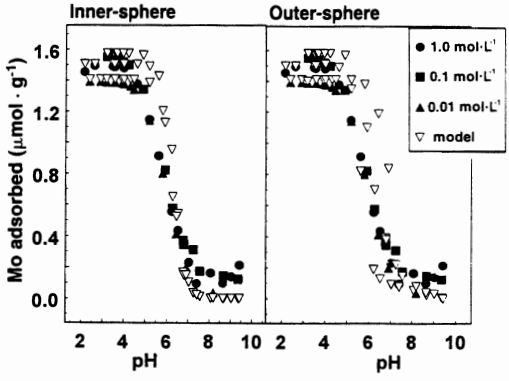

Figure 12 Molybdate adsorption on Porterville soil as a function of solution pH and ionic strength. Filled symbols represent experimental data. Triple-layer model results are represented by open triangles. $V_Y = 176$ for inner-sphere adsorption and $V_Y = 207$ for outer-sphere adsorption.

ner-sphere adsorption mechanism, only two adjustable parameters were optimized, the molybdate surface complexation constants. This number of adjustable parameters, again, compares very favorably with the empirical Langmuir and Freundlich adsorption isotherm approach. For all other materials we optimized the surface complexation constants for Na^+ and Cl^- along with the molybdate surface complexation constants, increasing the number of adjustable parameters to four. The surface site density suggested by Davis and Kent (1990) for natural materials was found appropriate for modeling molybdate adsorption on a variety of oxides, clay minerals, and soils. The triple-layer model was able to simultaneously fit molybdate adsorption at several ionic strengths with one set of surface complexation constants.

Triple-layer modeling suggests an inner-sphere adsorption mechanism for goethite, gibbsite, kaolinite, and the soils, and an outer-sphere adsorption mechanism for montmorillonite. Lack of agreement between various indirect methodologies of inferring adsorption mechanisms—zero point of charge shifts, ionic strength effects, and surface complexation modeling—underscores the necessity for direct spectroscopic elucidation of adsorption mechanisms. It is best to obtain spectroscopic evidence for the presence of particular surface complexes prior to postulating them in surface complexation models.

The advantage of the constant capacitance model over the triple-layer model is its simplicity and small number of adjustable parameters. The advantage of the triple-layer model is its ability to describe ion adsorption as a function of solution

Table IV

Solids, Concentrations, and Intrinsic Surface Complexation Constants Obtained with the Triple-Layer Model

	Inner-sphere mechanism				Outer-sphere mechanism			
Solid	log K^1_{Mo}(int)	log K^2_{Mo}(int)	log K_{Na}(int)	log K_{Cl} (int)	log K^1_{Mo}(int)	log K^2_{Mo}(int)	log K_{Na}(int)	log K_{Cl} (int)
Goethite	7.28	3.82	−9.3	5.4	9.66	4.92	−9.3	5.4
δ-Al_2O_3	8.93	3.92	−9.3	5.4	11.76	5.38	−11.23	9.64
Gibbsite	9.26	0.52	−8.52	13.00	8.97	2.09	−6.87	8.11
KGa-1 kaolinite	5.01	−0.87	−7.48	10.08	7.23	−0.17	−37.20	4.58
SWy-1 montmorillonite	—[a]	−0.92	−6.47	9.66	—	−0.47	−6.47	1.77
Pachappa soil	—	−2.09	−9.3	5.4	12.08	−0.61	−9.3	5.4
Porterville soil	—	−1.49	−9.3	5.4	12.24	−0.13	−9.3	5.4

[a]No convergence.

ionic strength and to consider both inner-sphere and outer-sphere surface complexes. The user must weigh improved chemical reality against increased complexity.

In the IR study high concentrations of Mo had to be used due to limitations in instrument sensitivity. Unfortunately, at these high concentrations polymeric Mo species are present in solution and their adsorption on the oxide surface cannot be ruled out. The kinetics and equilibria for processes occurring as basic solutions of MoO_4^{2-} are acidified are very complex. The polymolybdate anions consist primarily of octahedral MoO_6 groups, so that the conversion of MoO_4^{2-} into polyanions requires an increase in coordination number. Polynuclear Mo^{VI} species contain seven and eight Mo atoms in solution, such as $Mo_7O_{24}^{6-}$ and $Mo_8O_{26}^{4-}$ (Cotton and Wilkinson, 1980). Three IR bands at 933, 885, and 835 cm^{-1} were observed for the aqueous Mo anionic species at 0.05 and 0.1 $mol \cdot L^{-1}$ (Fig. 13). Assignments of IR bands for polymolybdate anions are not available in the literature.

Molybdate sorbed at the interface of $Fe(OH)_3(a)$ and water exhibited two IR bands at 925 and 880 cm^{-1}, with greater band intensities for the higher initial 0.1 $mol \cdot L^{-1}$ Na_2MoO_4 concentration than for 0.05 $mol \cdot L^{-1}$ Na_2MoO_4 (Fig. 14). This is consistent with the higher sorption of Mo (975 $mmol \cdot kg^{-1}$) at 0.1 $mol \cdot L^{-1}$

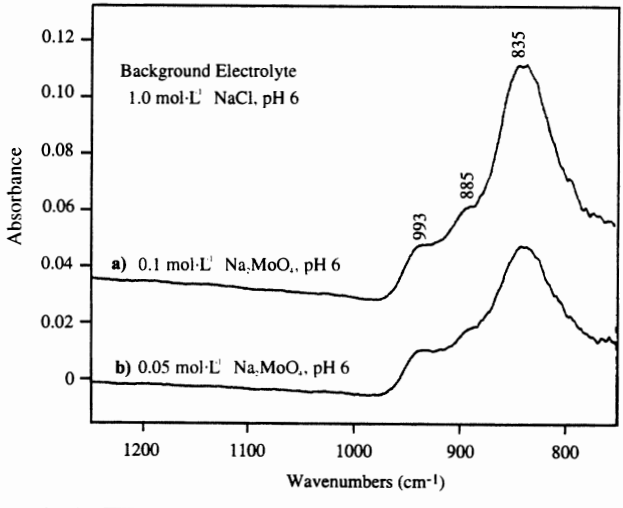

Figure 13 ATR-FTIR difference spectra of Na_2MoO_4 (pH 6) solutions: (a) 0.1 $mol \cdot L^{-1}$; (b) 0.05 $mol \cdot L^{-1}$. The reference spectrum was 1.0 $mol \cdot L^{-1}$ NaCl (pH 6).

Na_2MoO_4 compared to that at 0.05 mol·L^{-1} Na_2MoO_4 (499 mmol·kg^{-1}), corresponding to 99.1 and 99.9% of sorption of added Mo, respectively. The molar ratio of released OH to sorbed Mo was 1.36 at 0.1 mol·L^{-1} Na_2MoO_4 and 1.81 at 0.05 mol·L^{-1} Na_2MoO_4, suggesting a mixture of monodentate and bidentate species of complexed Mo at the mineral surface. It is evident that ligand exchange (inner-sphere complexation) is a mechanism for Mo sorption on $Fe(OH)_3$(a). X-ray diffractograms of $Fe(OH)_3$(a) after Mo sorption showed no crystalline solid phase. This microscopic result is in agreement with the macroscopic results obtained for the iron oxide, goethite, using zero point of charge shifts, ionic strength effects, and triple-layer modeling.

Two washings with deionized water desorbed 14 and 28% of the initially sorbed Mo from $Fe(OH)_3$(a) for the 0.05 and 0.1 mol·L^{-1} Na_2MoO_4 treatments, respectively. DRIFT difference spectra show that at least three IR bands can be identified in the range 1000 to 700 cm^{-1} for sorbed Mo (Figs. 15a and 15b). In com-

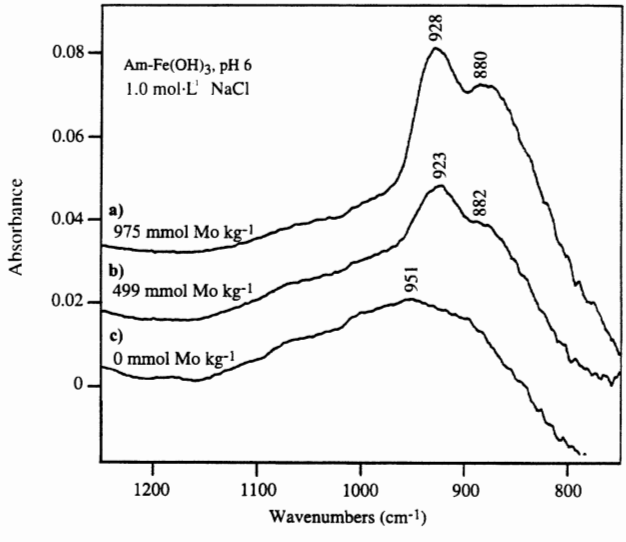

Figure 14 ATR-FTIR difference spectra of $Fe(OH)_3$(a) (the spectrum of the supernatant was subtracted from the spectrum of the solid suspension) as affected by Mo sorption. Solid concentration was 400 g·L^{-1}. The amount of sorbed Mo was (a) 975, (b) 499, and (c) 0 mmol·kg^{-1} of Mo for initial Mo concentrations of 0.1, 0.05, and 0 mol·L^{-1} Na_2MoO_4, respectively, in 1.0 mol·L^{-1} NaCl (pH 6).

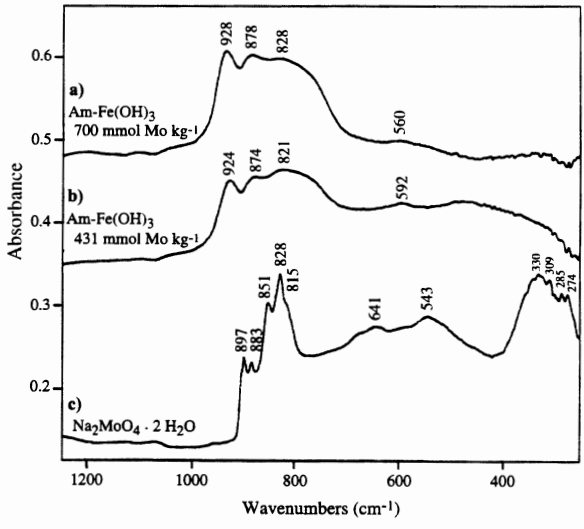

Figure 15 DRIFT difference spectra of Mo sorbed on $Fe(OH)_3$(a) after two washings with deionized water and air-drying: (a) 700 mmol·kg^{-1} of Mo for the initial 0.1 mol·L^{-1} Na_2MoO_4 treatment, and (b) 431 mmol·kg^{-1} of Mo for the initial 0.05 mol·L^{-1} Na_2MoO_4 treatment. (c) DRIFT spectrum of reagent-grade $Na_2MoO_4 \cdot 2H_2O$. All samples were diluted with KBr (5 mg in 95 mg KBr).

parison, more bands were observed for the reagent-grade $Na_2MoO_4 \cdot 2H_2O$ (Fig. 15c). A model monodentate complex $[Co(NH_3)_5MoO_4]Cl$ shows three IR bands at 910, 877, and 833 cm^{-1}, whereas a bidentate chelate $[Co(NH_3)_4MoO_4]NO_3$ exhibits four bands at 920, 868, 845, and 795 cm^{-1} (Ross, 1972). An estimation of the relative distribution of mono- and bidentate complexes is difficult due to overlapping bands of the complexes. Nevertheless, it is highly possible that both types of complexes exist on the surface of $Fe(OH)_3$(a), as supported by both IR spectra and the molar ratio of OH released to Mo sorbed.

IV. SUMMARY

Molybdate adsorption on all materials exhibited a maximum at low pH (3 to 5). With increasing solution pH, adsorption decreased rapidly, with little adsorption occurring above pH values of 7 to 8. Molybdate adsorption was lowest for the

highest solution ionic strength. Ionic strength dependence of molybdate adsorption was slight on goethite, montmorillonite, and soils, suggesting an inner-sphere adsorption mechanism. Ionic strength dependence of molybdate adsorption was obvious on gibbsite, Aluminium Oxid C, and kaolinite, suggesting an outer-sphere adsorption mechanism.

The constant capacitance model was able to describe molybdate adsorption on the oxides, clay minerals, and soils as a function of solution pH. Averages for the molybdate surface complexation constants obtained with the constant capacitance model for oxides, clay minerals, and soils were not statistically different at the 95% level of confidence.

The triple-layer model was able to describe molybdate adsorption on goethite, gibbsite, Aluminium Oxid C, kaolinite, montmorillonite, and two soils as a function of solution pH and ionic strength using a universal site density value of 2.31 sites·nm^2 (recommended for natural materials). Good fits of the model to the data were obtained using both inner-sphere and outer-sphere adsorption mechanisms for all materials except montmorillonite, where an acceptable fit was obtained only with an outer-sphere mechanism.

Results from the FTIR spectroscopy indicate that ligand exchange is a mechanism for Mo adsorption on amorphous iron hydroxide. Hydroxyl release suggests a mixture of monodentate and bidentate Mo surface complexes.

REFERENCES

Barrow, N. J. 1970. Comparison of the adsorption of molybdate, sulfate and phosphate by soils. *Soil Sci.* 109:282–288.

Bibak, A., and Borggaard, O. K. 1994. Molybdenum adsorption by aluminum and iron oxides and humic acid. *Soil Sci.* 158:323–327.

Carpéni, G. 1947. Sur la constitution des solutions aqueuses d'acide molybdique et de molybdates alcalins. IV.—Conclusions générales. *Bull. Soc. Chim.* 14:501–503.

Cihacek, L. J., and Bremner, J. M. 1979. A simplified ethylene glycol monoethyl ether procedure for assessing soil surface area. *Soil Sci. Soc. Am. J.* 43:821–822.

Coffin, D. E. 1963. A method for the determination of free iron oxide in soils and clays. *Can. J. Soil Sci.* 43:7–17.

Cotton, F. A., and Wilkinson, G. 1980. "Advanced Inorganic Chemistry," 4th ed., pp. 852–856. Wiley, New York.

Davis, J. A., James, R. O., and Leckie, J. O. 1978. Surface ionization and complexation at the oxide/water interface. I. Computation of electrical double layer properties in simple electrolytes. *J. Colloid Interface Sci.* 63:480–499.

Davis, J. A., and Kent, D. B. 1990. Surface complexation modeling in aqueous geochemistry. *Rev. Mineral.* 23:117–260.

Ferreiro, E. A., Helmy, A. K., and de Bussetti, S. G. 1985. Molybdate sorption by oxides of aluminium and iron. *Z. Pflanzenernaehr. Bodenk.* 148:559–566.

Goldberg, S., Forster, H. S., and Godfrey, C. L. 1996. Molybdenum adsorption on oxides, clay minerals, and soils. *Soil Sci. Soc. Am. J.* 60:425–432.

Goldberg, S., and Sposito, G. 1984a. A chemical model of phosphate adsorption by soils. I. Reference oxide minerals. *Soil Sci. Soc. Am. J.* 48:772–778.

Goldberg, S., and Sposito, G. 1984b. A chemical model of phosphate adsorption by soils. II. Noncalcareous soils. *Soil Sci. Soc. Am. J.* 48:779–783.

Gonzalez, B. R., Appelt, H. Schalscha, E. B., and Bingham, F. T. 1974. Molybdate adsorption characteristics of volcanic-ash-derived soils in Chile. *Soil Sci. Soc. Am. Proc.* 38:903–906.

Hayes, K. F., and Leckie, J. O. 1987. Modeling ionic strength effects on cation adsorption at hydrous oxide/solution interfaces. *J. Colloid Interface Sci.* 115:564–572.

Hayes, K. F., Papelis, C., and Leckie, J. O. 1988. Modeling ionic strength effects on anion adsorption at hydrous oxide/solution interfaces. *J. Colloid Interface Sci.* 125:717–726.

Herbelin, A. L., and Westall, J. C. 1994. FITEQL: A computer program for determination of chemical equilibrium constants from experimental data. Rep. 94-01, Version 3.1, Dept. of Chemistry, Oregon State University, Corvallis, OR.

Jarrell, W. M., and Dawson, M. D. 1978. Sorption and availability of molybdenum in soils of western Oregon. *Soil Sci. Soc. Am. J.* 42:412–415.

Jones, L. H. P. 1957. The solubility of molybdenum in simplified systems and aqueous soil suspensions. *J. Soil Sci.* 8:313–327.

Karimian, N., and Cox, F. R. 1978. Adsorption and extractability of molybdenum in relation to some chemical properties of soil. *Soil Sci. Am. J.* 42:757–761.

Klages, M. G., and Hopper, R. W. 1982. Clay minerals in northern plains coal overburden as measured by x-ray diffraction. *Soil Sci. Soc. Am. J.* 45:415–419.

Kyle, J. H., Posner, A. M., and Quirk, J. P. 1975. Kinetics of isotopic exchange of phosphate adsorbed on gibbsite. *J. Soil Sci.* 26:32–43.

Kyriacou, D. 1967. The pH-dependence of adsorption of metallic oxyanions by ferric oxide powder. *Surf. Sci.* 8:370–372.

Lindsay, W. L. 1979. "Chemical Equilibria in Soils." Wiley, New York.

McKenzie, R. M. 1983. The adsorption of molybdenum on oxide surfaces. *Aust. J. Soil Res.* 21:505–513.

McLaughlin, J. R., Ryden, J. C., and Syers, J. K. 1981. Sorption of inorganic phosphate by iron and aluminium-containing components. *J. Soil Sci.* 32:365–377.

Mikkonen, A., and Tummavuori, J. 1993a. Retention of vanadium(V), molybdenum(VI) and tungsten(VI) by kaolin. *Acta Agric. Scand. Sect. B Soil Plant Sci.* 43:11–15.

Mikkonen, A., and Tummavuori, J. 1993b. Retention of molybdenum(VI) by three Finnish mineral soils. *Acta Agric. Scand. Sect. B Soil Plant Sci.* 43:206–212.

Motta, M. M., and Miranda, C. F. 1989. Molybdate adsorption on kaolinite, montmorillonite, and illite: Constant capacitance modeling. *Soil Sci. Soc. Am. J.* 53:380–385.

Murphy, L. S., and Walsh, L. M. 1972. Correction of micronutrient deficiencies with fertilizers. *In* "Micronutrients in Agriculture" (J. H. Mortvedt, P. M. Giordano, and W. L. Lindsay, Eds.). Soil Science Society of America, Madison, WI.

Nelson, D. W., and Sommers, L. E. 1982. Total carbon, organic carbon, and organic matter. *In* "Methods of Soil Analysis" (A. L. Page *et al.*, Ed.), 2nd ed., Part 2, Chap. 9, pp. 539–579. American Society of Agronomy, Madison, WI.

Phelan, P. J., and Mattigod, S. V. 1984. Adsorption of molybdate anion (MoO_4^{2-}) by sodium-saturated kaolinite. *Clays Clay Miner.* 32:45–48.

Reisenauer, H. M., Tabikh, A. A., and Stout, P. R. 1962. Molybdenum reactions with soils and the hydrous oxides of iron, aluminum and titanium. *Soil Sci. Soc. Am. J.* 26:23–27.

Reyes, E. D., and Jurinak, J. J. 1967. A mechanism of molybdate adsorption on αFe_2O_3. *Soil Sci. Soc. Am. J.* 31:637–641.

Ross, S. D. 1972. "Inorganic Infrared and Raman Spectra," p. 217. McGraw-Hill, London.

Roy, W. R., Hassett, J. J., and Griffin, R. A. 1986. Competitive interactions of phosphate and molybdate on arsenate adsorption. *Soil Sci.* 142:203–210.

Roy, W. R., Hassett, J. J., and Griffin, R. A. 1989. Quasi-thermodynamic basis of competitive-adsorption coefficients for anionic mixtures in soils. *J. Soil Sci.* 40:9–15.

Spanos, N., and Lycourghiotis, A. 1995. Codeposition of $Mo^{(VI)}$ species and Ni^{2+} ions on the γ-alumina surface: Mechanistic model. *J. Colloid Interface Sci.* 171:306–318.

Spanos, N., Vordonis, L., Kordulis, Ch., and Lycourghiotis, A. 1990a. Molybdenum-oxo species deposited on alumina by adsorption. I. Mechanism of the adsorption. *J. Catal.* 124:301–314.

Spanos, N., Vordonis, L., Kordulis, Ch., Koutsoukos, P. G., and Lycourghiotis, A. 1990b. Molybdenum-oxo species deposited on alumina by adsorption. II. Regulation of the surface Mo^{VI} concentration by control of the protonated surface hydroxyls. *J. Catal.* 124:315–323.

Sposito, G. 1984. "The Surface Chemistry of Soils." Oxford University Press, New York.

Sprycha, R. 1989a. Electrical double layer at alumina/electrolyte interface. I. Surface charge and zeta potential. *J. Colloid Interface Sci.* 127:1–11.

Sprycha, R. 1989b. Electrical double layer at alumina/electrolyte interface. II. Adsorption of supporting electrolytes. *J. Colloid Interface Sci.* 127:12–25.

Stumm, W., Kummert, R., and Sigg, L. 1980. A ligand exchange model for the adsorption of inorganic and organic ligands at hydrous oxide interfaces. *Croat. Chem. Acta* 53:291–312.

Su, C., and Suarez, D. L. 1995. Coordination of adsorbed boron: A FTIR spectroscopic study. *Environ. Sci. Technol.* 29:302–311.

Theng, B. K. G. 1971. Adsorption of molybdate by some crystalline and amorphous soil clays. *New Zealand J. Sci.* 14:1040–1056.

Vordonis, L., Koutsoukos, P. G., and Lycourghiotis, A. 1990. Adsorption of molybdates on doped γ-aluminas in alkaline solutions. *Colloids Surf.* 50:353–361.

Westall, J., and Hohl, H. 1980. A comparison of electrostatic models for the oxide/solution interface. *Adv. Colloid Interface Sci.* 12:265–294.

Xie, R. J., and MacKenzie, A. F. 1991. Molybdate sorption-desorption in soils treated with phosphate. *Geoderma* 48:321–333.

Xie, R. J., MacKenzie, A. F., and Lou, Z. J. 1993. Causal modeling pH and phosphate effects on molybdate sorption in three temperate soils. *Soil Sci.* 155:385–397.

Zhang, P. C., and Sparks, D. L. 1989. Kinetics and mechanisms of molybdate adsorption/desorption at the goethite/water interface using pressure-jump relaxation. *Soil Sci. Soc. Am. J.* 53:1028–1034.

Zhang, P., and Sparks, D. L. 1990. Kinetics of selenate and selenite adsorption/desorption at the goethite/water interface. *Environ. Sci. Technol.* 24:1848–1856.